

From ramp to platform: building a 3D model of depositional geometries and facies architectures in transitional carbonates in the Miocene, northern Sardinia

Sara Tomás · M. Zitzmann · M. Homann ·
M. Rumpf · F. Amour · M. Benisek ·
G. Marcano · M. Mutti · C. Betzler

Received: 22 February 2009 / Accepted: 29 October 2009
© Springer-Verlag 2009

Abstract The depositional geometry and facies distribution of an Early Miocene (Burdigalian) carbonate system in the Perfugas Basin (NW Sardinia) comprise a well-exposed example of a transition from a ramp to a steep-flanked platform. The carbonate succession (Sedini Limestone Unit) is composed of two depositional sequences separated by a major erosional unconformity. The lower (sequence 1) records a ramp dominated by heterozoan producers and the upper (sequence 2) is dominated by photozoan producers and displays a gradual steepening of the depositional profile into a steep-flanked platform. This paper shows the process of creating a digital outcrop model including a facies model. This process consists of combining field data sets, including 17 sedimentary logs, and a spatial dataset consisting of differential global positioning system data points measured along key stratigraphic surfaces and sedimentary logs, with the goal of locking traditional field observations into a 3D spatial model. Establishing a precise geometrical framework and visualizing the overall change in the platform geometry and the related vertical and lateral facies variations of the Sedini carbonate platform, allows us to better understand the sedimentary processes leading to the geometrical turn-over of the platform. Furthermore, a

detailed facies modeling helps us to gain insight into the detailed depositional dynamics. The final model reproduces faithfully the depositional geometries observed in the outcrops and helps in understanding the relationships between facies and architectural framework at the basin scale. Moreover, it provides the basis to characterize semiquantitatively regional sedimentological features and to make further reservoir and subsurface analogue studies.

Keywords Digital outcrop model (DOM) · Geometry · Facies distribution · Transitional carbonates · Sardinia

Introduction

Reconstruction of geometries of carbonate depositional systems and their internal facies distribution is essential for a better understanding of lateral and vertical heterogeneity, complex stacking patterns, and stratal anatomy (Bosence et al. 1998; Bosence 2005; Warlich et al. 2005; Asprien et al. 2008). The investigation of the type and loci of carbonate production, as well as of the factors controlling the depositional geometries and facies distribution (sea-level and paleoceanographic fluctuations or climate; Pomar and Kendall 2007; Pomar and Hallock 2008) are of wide interest. The reconstruction of depositional models in spatial dimensions by means of integrating quantitative field studies with digital outcrop models (DOMs) is proving a new development to traditional field studies. This new spatial representation of traditional observations is an important tool that helps to gain new insights to extract depositional geometries and facies architectures and information that are otherwise unobtainable. The use of digital models of outcrop analogues has long been acknowledged by subsurface reservoir modelers (Grammer

S. Tomás (✉) · M. Zitzmann · M. Homann · M. Rumpf ·
F. Amour · G. Marcano · M. Mutti
Institute of Geosciences, University Potsdam, Potsdam,
Germany
e-mail: stomas@geo.uni-potsdam.de

M. Benisek
StatoilHydro ASA, Forushagen, Stavanger, Norway

C. Betzler
Institute of Geology and Paleontology,
University Hamburg, Hamburg, Germany

et al. 2004; Pringle et al. 2006; Enge et al. 2007; Jones et al. 2007; Redfern et al. 2007; Verwer et al. 2007; references therein; Fabuel-Perez 2008). Outcrop analogues need to be geologically comparable to the studied system in the subsurface and also need excellent 3D outcrop exposures over an area large enough to capture the scale required (Clark and Pickering 1996). Therefore, the utilization of outcrop studies, which allow 3D observations at many different scales, is commonly used to reduce the uncertainty associated with interpreting subsurface data.

However, despite the outstanding quality of some outcrops, the natural physical limitations such as their large dimensions, localized exposures within the regional framework, or inaccessibility, may also make the establishment of a precise geometrical framework difficult. Modeling provides a tool to improve the continuity and connectivity of field observations across a regional framework in the locations where data collection is limited. Therefore, it is important to collect in the field a grid of horizontal and vertical data points, with survey technologies, such as differential global positioning systems (DGPS) or a terrestrial laser scan (LIDAR; e.g., Adams et al. 2004, 2005; Verwer et al. 2004; Bellian et al. 2005), which spatially define the geometrical framework. Clearly, the 3D data are useful only if they are supported by a detailed field interpretation of geometries, surface hierarchies, and facies distribution.

The Miocene of northern Sardinia provides a very good setting to test the methods of integrating field and DOM studies in a location characterized by good outcrop quality at basin scale, but not connected physically throughout the basin. The system is characterized by a mixture of photozoan and heterozoan biotic assemblages (transitional carbonates, according to Halfar et al. 2004). This setting records a vertical transition from a lower heterozoan-dominated ramp to an upper photozoan-dominated steep-flanked platform. During the last decades, many contributions have specifically dealt with temperate and subtropical carbonate systems of the Miocene in the Mediterranean (e.g., Esteban 1996; Martín et al. 1996; Betzler et al. 1997, 2000; Brachert et al. 1996, 1998; Mutti et al. 1997) and have sparked debate concerning whether these are directly related to climatic belts/water temperature or to other environmental factors (Mutti et al. 1999; Brandano and Corda 2002; Pomar et al. 2004; Brandano et al. 2005). Little is also known about the depositional geometries of these carbonate systems, intermediate between the two end-member geometries (ramp to steep-flanked platform) and about the relationships to the main controlling factors.

Previous studies in the Perfugas Basin have provided a detailed sedimentological and stratigraphical model and have documented the turnover from the ramp into the steep-flanked platform as well as the relationships among facies types, biotic assemblages, and the stratigraphic architecture

(Benisek 2008; Benisek et al. 2009b). Despite the outstanding quality of the outcrops at the basin scale, localized inaccessibility due to cliffs or lack of physical connections among outcrops make the use of a DOM crucial. By using the previous field-based studies as the sedimentological and stratigraphical framework, combined with the acquisition of a new spatial grid of horizontal and vertical data points, the aim of the present work is the generation of a 3D geological model that permits to understand the architecture of the different stages of platform evolution and their relationship with facies distribution. This paper also sets an example of digital outcrop modeling of carbonate systems, focusing on the methodology and workflow used to create these models. Furthermore, it discusses the limitations of reconstructing facies distribution in large-scale.

Geological setting

The studied Miocene (Burdigalian) deposits crop out in the Perfugas Basin, an extensional basin located 10–30 km east of the city of Sassari, in northern Sardinia (Fig. 1a). During the Oligo-Miocene, marine carbonates, siliciclastics, lacustrine and volcanic deposits accumulated in the Perfugas Basin, which consists of a half-graben bounded by preferentially oriented NW–SE faults with vertical offsets of up to 40 m. The Oligo-Miocene succession can be subdivided into stages of rift and post-rift development, accompanied by extensive volcanism, as result of the counter-clockwise rotation of the Corsica-Sardinian block (Cherchi and Montadert 1982) due to the opening of the Balearic and Ligural-Provencal Basin (Schettino and Turco 2006). This extensive rift-drift regime continues until present times. In the Perfugas Basin, marine conditions predominated during the Mid-Late Burdigalian and prograding fault-block shallow-water carbonate platforms, up to 60 m thick, accumulated. Part of these deposits crop out between the villages of Sedinì, Laerru, and Perfugas, covering an area of about 18 km² (Sedinì carbonate platform). The Burdigalian post-rift marine carbonate succession of the Sedinì Limestone Unit (Thomas and Gennesseaux 1986) varies from 10 to 60 m in thickness and overlies alluvial basal conglomerates, volcanoclastics and lacustrine sediments of the Perfugas Formation (Sowerbutts 2000), which onlaps the volcanic substrate of the Tergu Formation (Fig. 2).

Stratigraphic architecture and sedimentology of the Sedinì carbonate platform

Stratigraphic architecture

The overall stratigraphic architecture and internal facies distribution of the Sedinì Limestone Unit have been

Fig. 1 Location of the studied area and transects. **a** Geological map of the Perfugas Basin, in northwest Sardinia. Modified from Thomas and Genesseeux (1986). The box depicts the location of the study area. **b** Schematic map showing the location of the studied transects and the measured stratigraphic sections

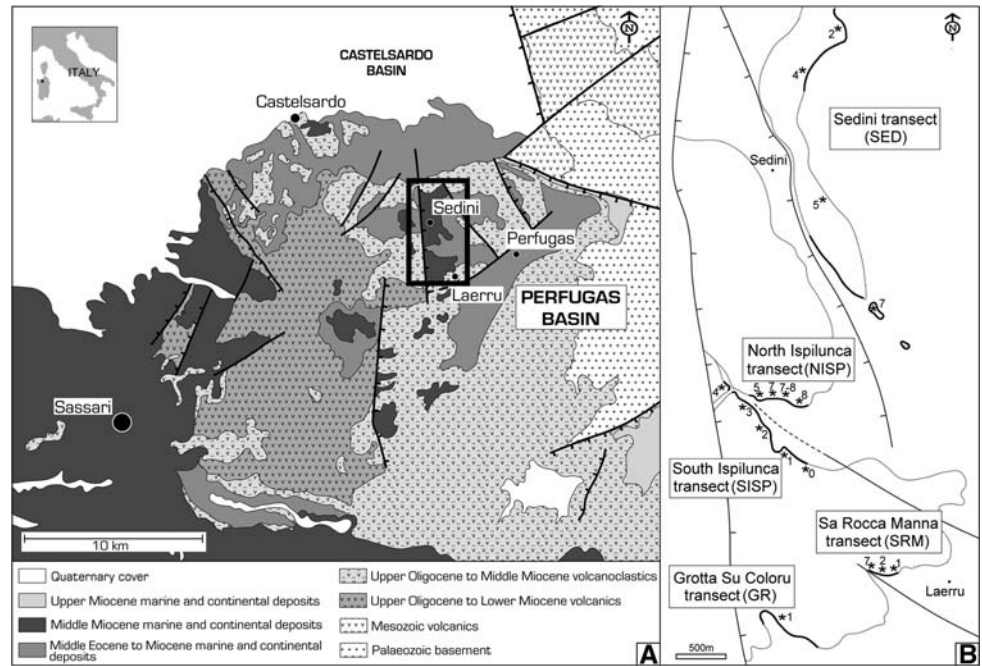
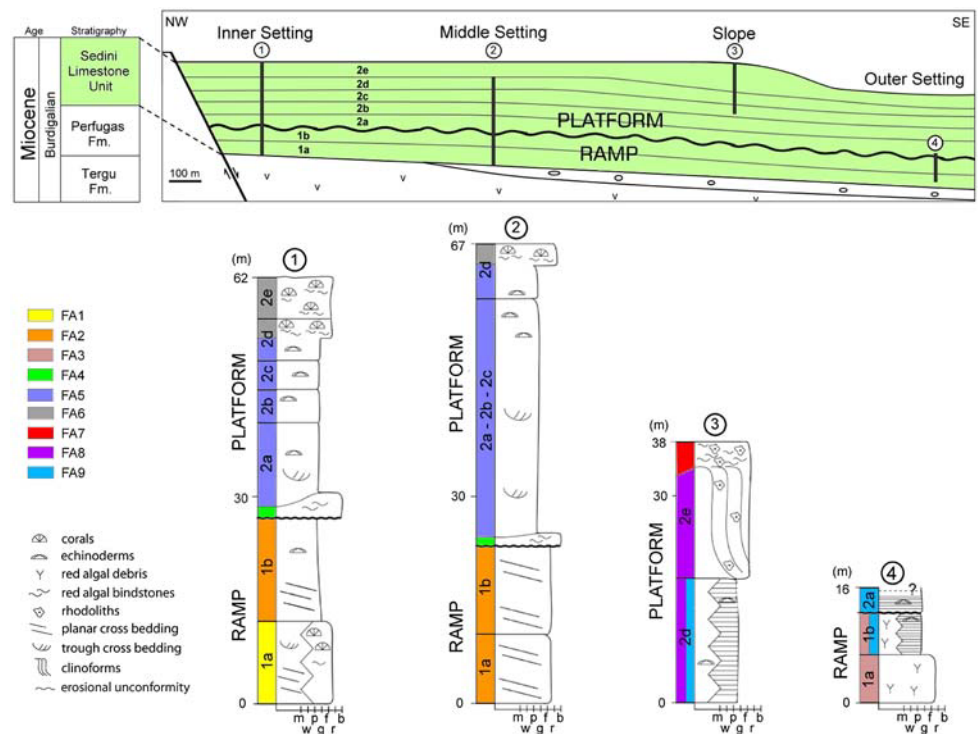


Fig. 2 Stratigraphic architecture and sedimentology of the study area. *Top* the Sedini Limestone unit (Burdigalian in age) shows a ramp depositional profile (sequence 1) changing into a steep-flanked platform (sequence 2) separated by a major erosional unconformity. Note the interpreted subsequences (1a–1b in the ramp and 2a–2e in the platform). *Bottom* synthetic stratigraphic sections showing the facies associations (FA) along the ramp and platform depositional profiles, from inner (1) to outer (4) settings



previously analyzed in detail by Benisek et al. (2009a, 2009b). Herein only a brief summary of the field data is provided and the reader is referred to these articles for a detailed overview. Benisek et al. (2009a, 2009b) identify two depositional sequences (sequences 1 and 2) in the Sedini Limestone Unit; both sequences are separated by a major erosional unconformity (Fig. 2). Sequence 1 records

a heterozoan-dominated homoclinal ramp system that is interpreted to have been deposited in an embayment opening to the SE (Benisek et al. 2009b). Sequence 2 shows a gradual change of the depositional profile into a photozoan-dominated steep-flanked platform system. Each sequence can be internally subdivided into different subsequences: two in sequence 1 (1a–1b) and five in sequence

2 (2a–2e; Benisek et al. 2009b), separated by minor erosional surfaces. These key surfaces can be traced physically across the area and are used as the horizons that provide the geometrical framework needed to create the geocellular model (see below).

Sedimentology and facies associations

To create the geological framework of the digital outcrop model, five transects have been selected: Sedin (SED), North Ispilunca (NISP), South Ispilunca (SISP), Sa Rocca Manna (SRM), and Grotta Su Coloru (GR; Fig. 1b). Each of these transects captures at least one significant facies transition within the Sedin Limestone Unit. The detailed analysis of the sedimentology and interpretation of facies of the Sedin carbonate platform has been done by Benisek (2008) and Benisek et al. (2009b), and will provide the framework on which this model is based. These authors identified 16 facies types. In order to take into account computational limitations and the size of model cells (see later discussion), all the facies types occurring in packages thinner than 1 m have been discarded. This makes a total of 13 facies types, which have been grouped into nine facies associations (FA), defined on the basis of their environment of deposition. These facies are outlined in Table 1 and Fig. 2 and are only briefly discussed below. They represent lateral and vertical evolution stages of this carbonate system.

Inner ramp fringing reefs and beaches (FA1)

The inner ramp facies vary from floatstones to rudstones containing branching red algae, bivalves, bryozoans, and coral fragments in the northern part (SED transect) to cross-bedded echinoid grainstones and packstones with bivalve debris in the south (GR transect). The first facies type forms small fringing reefs which interfinger with floatstones and rudstones with branching red algae. The second facies type is characterized by low-angle, planar cross-bedded deposits that pass laterally into medium-scale trough cross-bedded deposits. This lateral facies variation is typical for a beach depositional system (see Benisek et al. 2009b), where the planar cross bedding indicates sedimentation in the foreshore area and the trough cross bedding represents the shoreface area.

Middle ramp longshore bars (FA2)

These facies consist of floatstones and rudstones with coralline red algal debris, rhodoliths, and the large benthic foraminifera *Amphistegina* sp. and *Heterostegina* sp. They show large-scale planar cross bedding with straight foresets and constant directions and angles of 15°. The cross-bedded bodies are approximately 9 m thick and extend laterally up to a few hundred meters. In the NISP and SISP transects, the cross bedding is present throughout the area, whereas in the SED transect this structure occurs just locally.

Table 1 Overview of the facies associations (FA) of the Sedin Limestone Unit and their most important characteristics

FA	Facies ^a	Texture	Geometry	Main components	Dep. environment	Transects
1	1	Float-Rudstone	Patches	Red algae, corals	Inner ramp	SED
	2	Pack-Grainstone	Cross beds	Echinids		GR
2	5	Float-Rudstone	Planar cross beds	Branching red algae, LBF	Middle ramp	NISP, SISP
						SED
3	4	Float-Rudstone	Massive	Red algae, LBF	Middle-outer ramp	SED, NISP
	7	Pack-Floatstone	Bedded	Red algae		SISP
4	3	Bindstone	Lenses	Red algae	Inner-middle platform (E-M)	NISP, SISP
	7					SRM
5	12	Pack-Grainstone	Planar cross beds	Red algae, echinids, LBF	Inner-middle platform (E-M)	NISP, SISP
						SRM
6	9	Boundstone	Reef flat	Corals	Inner platform (L)	NISP, SISP
	11	Rud-Bindstone	Lenses	Corals, red algae		SRM
7	13	Float-Rudstone	Inclined beds	Echinids, corals	Incipient slope	SRM
	14	Float-Rud-Bindst.		Red algae, rhodoliths		Slope break (L)
8	15	Rudstone	Clinoforms	Rhodoliths	Slope (L)	SRM
9	16	Wack-Packstone	Bedded	Echinids, bivalves, planktic forams	Outer ramp and outer platform	SED, NISP, SISP, SRM

LBF large benthic foraminifera, *E-M* early-middle stages of platform evolution, *L* latest stage of platform evolution

^a Facies types from Benisek (2008)

Middle-outer ramp deposits (FA3)

This association is well exposed in the SED transect and is characterized by coralline red algal debris floatstones and rudstones that pass vertically into wackestones and packstones mainly consisting of coralline red algal debris and echinoids. Both types of facies contain the large benthic foraminifera *Amphistegina* sp. and *Heterostegina* sp., bivalve fragments and bryozoans.

Inner-middle platform red algal bindstones (FA4)

These bindstones form lenses up to 4 m thick and a few hundred meters long and contain encrusting coralline red algae, bivalves, and echinoids. During the early-middle stages of platform evolution they occur in inner and middle platform settings characterized by low hydrodynamic conditions. They form locally lenses in the deposits of FA5 (explained below) and crop out in NISP, SISP, and SRM transects.

Inner-middle platform bioclastic packstones and grainstones (FA5)

Packstones and grainstones containing branching red algae, echinoids, and foraminifera (*Heterostegina* sp. and *Amphistegina* sp.) characterize the inner-middle platform environments. These deposits often show large-scale, low-angle trough cross-bedding structures that are interpreted as submarine dunes and form bodies 12 m thick and 70–100 m long. The dunes create a subtle topography forming the incipient platform margin during the early-middle stages of platform growth. These deposits crop out in the NISP, SISP, and SRM transects.

Inner platform bioconstructions (FA6)

Two different facies types, which pass vertically and laterally one into the other, characterize the inner platform top during the latest stage of platform growth: coral framestones and coralline red algal bindstones. In the innermost part of the platform top, the framestones form build-ups of ~6 m height and 100 m width. Beds, up to 5 m thick and 200 m wide, of coralline red algal bindstones underlie the coral build-ups. Basinward, towards the platform margin, the red algal bindstones become gradually more abundant and the coral framestones disappear. FA6 is well exposed in SISP and SRM transects.

Slope break area and incipient slope (FA7)

The slope of the platform was developed during the latest stage of the platform growth. The slope break and slope deposits crop out in the SRM and SISP transects and are

interpreted as fore-reef deposits on the basis of their distal continuity with the inner platform top (FA6). The detailed characterization of the slope deposits has been possible due to the excellent exposure in the SRM transect. Two different facies types characterize FA7. The first type consists of floatstones and rudstones with echinoids, bivalves, and coral debris formed at the beginning of the development of the slope geometry. This facies shows large-scale planar cross beds dipping slightly basinwards. The second type includes coralline red algal bindstones mixed with rhodolith floatstones and rudstones that form the topset deposits of the slope clinofolds (explained below).

Platform slope clinofolds (FA8)

Steep clinofolds characterize the advanced stage of slope development. These deposits are formed by rhodolith rudstones and crop out in the SISP and SRM transects. The clinofolds are arranged in 20-m-high strata dipping basinwards up to 27°. The rhodolith rudstones are laterally continuous with the FA7.

Outer ramp and outer platform (FA9)

These deposits are formed by well-bedded and bioturbated wackestones and packstones with echinoids, bivalves, small planktic foraminifers, and glauconite. Their exposure is very limited. They crop out in the NISP, SISP, and SRM transects, and in the central-west part of the Sedini area.

Materials and methods

The basic stratigraphic sections and field interpretations of key stratigraphic surfaces done by Benisek (2008) and Marcano (2008) have been supplemented by a collection of additional stratigraphic sections and photo panoramas combined with differential global positioning (DGPS) data. The DGPS data on surfaces and sections provide the framework to build the digital outcrop model.

Spatial data acquisition and instrumentation

A spatial data set was collected using a DGPS. In total approximately 7 km of tracked surfaces were measured, with 1 data point per 1 m distance. Each data point records XYZ position information. Measurements were taken along stratigraphic surfaces and vertical stratigraphic sections. The spatial resolution of each data point is expressed by its 3D quality factor, which defines the accuracy of the positioning of each point in the 3D space. 3D quality factors are strongly dependent on the number of satellites available for positioning, which at the same time depends

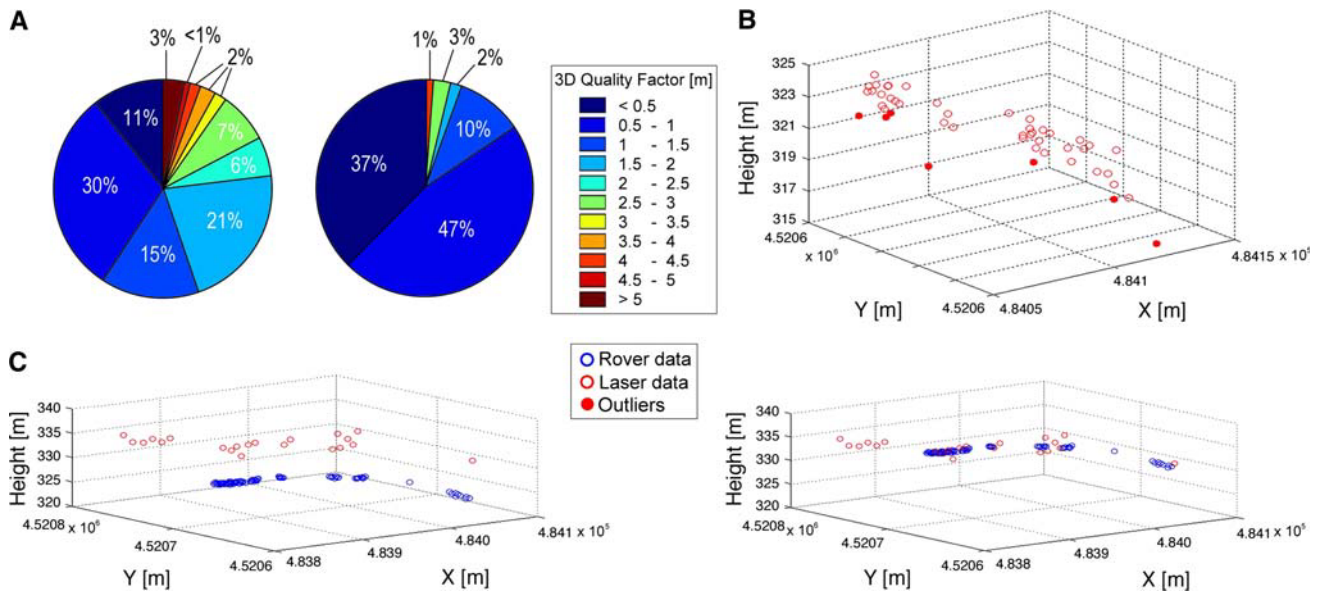


Fig. 3 Processing of the spatial data. **a** Pie charts showing the 3D quality factors of the rover data set, before (*left*) and after (*right*) removal of outliers. The 3D quality factors are grouped into intervals. The amount of data (in percentage) included in these different intervals is shown. Note that after data correction most of the rover data measurements (84%) show an accuracy of <1 m. **b** 3D plot of the

spatial coordinates of a laser data set measured at one specific outcrop and date, showing both outliers and reliable measurements. **c** 3D plots of the spatial coordinates of a rover and a laser data set measured in one outcrop, before (*left*) and after (*right*) the adjustment of the laser data to the rover data, due to the higher accuracy of the latter

on the terrain topography and the weather condition of the surveyed area. In the present work the 3D quality factors vary between 30 cm and 5 m (Fig. 3a).

A real-time kinematic differential global positioning system (DGPS) was used to collect 3D data. The system consists of two receivers (LEICA GPS 1200), that operate both as a DGPS while interconnected via radio communication. One of these two receivers acts as a fixed base station and provides real-time correction data for the second receiver (rover). In accessible outcrop sectors, georeferenced points were measured every meter by physically walking along the key stratigraphic surfaces. Also, measurements were acquired on the stratigraphic sections to get some vertical control points. This was possible whenever the thickness of the measured bed was larger than the spatial resolution given by the 3D quality factor (30 cm to 5 m). If outcrop sectors were inaccessible, it was necessary to use a different instrument, the laser locator. The laser locator measures distances and vertical angles from a specific position to the outcrop. This position needs to be referenced by using the rover. The measured data were directly stored in real-world coordinates by combining with measured rover positions. Measured distances for the laser locator varied from 10 to 600 m and measurement angles between 0° and 5°.

Data processing

In order to improve the quality/reliability of the DOM, the acquired spatial data needed to be processed. For this

purpose, all the data points above a certain Euclidian norm distance (Z dimension) from the general trend of the data points were considered unreliable (outliers) and were therefore excluded. Two different techniques were applied to rule out outliers depending on the instrument (rover or laser locator) used to acquire the data. The points measured with the rover show a broad range of 3D quality factors due to the variable reception of satellites at the different measurement positions. Therefore, it was necessary to correct the data for each position separately. The mean value of all 3D quality factors was computed and all those points whose factor differed from the mean more than one standard deviation were removed (Fig. 3a). The laser measurements taken from a same reference position have the same 3D quality factor, since this factor expresses the accuracy of spatial positions and the laser locator just measures distances and angles from a position of reference (Fig. 3b). Therefore, the 3D quality factor is not taken into account to remove outliers from the laser data sets. These outliers result directly from measurement imprecision and weather condition and are visualized and removed by logical reasoning, i.e., the points with the largest offsets (Z dimension) from the general trend of the data points (Fig. 3b). Once outliers were excluded from the rover and the laser data sets separately, it was necessary to adjust the offset (Z dimension) between both data sets. To calibrate the two data sets several measurements were taken from a same position with both instruments the rover and the laser locator. The Z coordinate of the laser data points was

adjusted to that of the rover data points, which was considered more precise. For this purpose, a linear relationship coming out from the calibration of rover and laser data sets was used (Fig. 3c).

Modeling workflow

The workflow used for the construction of the digital outcrop model includes: (1) creation of a geocellular model and (2) generation of a facies model.

Geocellular modeling

Firstly, the digital elevation model (DEM) of the study area and the processed spatial data (explained above) were imported into a software package (PETREL-Schlumberger trademark) as a series of points (Fig. 4a–c). The DEM of the area has a resolution of 10 m. Fault traces were created by reproducing their orientation (NW–SE) and vertical offset (40–50 m) and then digitized to generate three-dimensional fault planes (Fig. 4f). Subsequently, the *X* and *Y* dimensions of the individual cells forming the geocellular model were defined (“gridding” process). The size of the cells was set to 10 × 10 m (*X*–*Y* dimensions) so it reflects the horizontal variation observed in the study area. This cell size offers a compromise between resolution and computational time (Fig. 4e). Finally, the vertical cell size is determined by creating horizons, zones, and layers. Horizons represent the interpreted key stratigraphic surfaces and were generated by using a minimum curvature interpolation algorithm (Fig. 4d). Zones are then defined as the interval between two successive mapped horizons, which corresponds to a stratigraphic subsequence (Fig. 4d). Finally, the zones were divided into equally spaced (1 m thick) layers, which represent an adequate resolution to reflect the facies variations. The final geocellular model is 6.6 km long, 2.5 km wide, and 130 m thick, and contains a total number of 52,102,908 cells, each 10 m × 10 m × 1 m (*X*, *Y*, *Z*).

Facies modeling

Firstly, the raw log data, providing detailed facies distribution at discrete locations, are imported into the software. The raw logs have to be georeferenced, positioning their base, and top. Secondly, raw log data were upscaled (Fig. 5) by assigning a particular code to each facies association so each cell of the geocellular model is intersected by each log (Fig. 5).

In order to build the 3D geological facies model, a stochastic approach, which permits to build realistic equiprobable facies distributions (Falivene et al. 2006 and references therein), was followed. To obtain the most

realistic facies model of the outcrop, two different modeling algorithms were applied, Sequential Indicator Simulation (SIS) and Truncated Gaussian Simulation (TGS). Each zone (stratigraphic subsequence) in the model was modeled separately. The modeling process was iterative, trying to create a model that matches the interpretations made in the field and similar geological scenarios.

In order to populate the model area with facies associations (FA), it is necessary to define some conditioning parameters (e.g., facies proportions, variograms, and object parameters, see Falivene et al. 2006). For this model, the vertical facies proportions, which correspond to the percentage of each facies association in each layer of the model, are obtained directly from the upscaled logs.

Results

Modeling the architecture of the carbonate system by the deterministic reconstruction of stratigraphic boundaries and by the stochastic population of facies heterogeneity creates a virtual continuity among all the discrete locations studied in the field by interpolation processes. This has allowed the better understanding of the depositional geometries and their relationships to facies distribution in each evolutionary stage of the studied platform.

Depositional geometry: reconstructed model versus outcrop data

The stratigraphic architecture of the carbonate system reconstructed by the model matches well with the geometries observed in the field. The 3D model allows an immediate visual overview of the dimensions of the studied carbonate system: 6.6 km in length, 3.3 km in width, and 130 m in thickness.

However, it is worth mentioning that the model reconstructs both the outcropping and non-outcropping sectors of the successions, giving rise to some thickness overestimation. Therefore, in order to assess the real thickening and thinning trends of the carbonate platform, it is important to consider this problem. These thickness artefacts are mostly observed where the upper or lower boundaries of the subsequences were not observed in the field, since the model extends the upper boundary of the zone upwards until the top of the DEM (e.g., subsequence 1b in the Sedini transect) or the lower boundary of the zone downwards until the base of the model (e.g., subsequence 1a in the Ispilunca transects). The variations in thickness reconstructed for the ramp deposits (sequence 1) do not show a clear orientated depositional trend. The thickest succession encompassing subsequences 1a and 1b is 30 m, and crops out in the SW of the study area (GR transect) whereas in

the NE part (SED 5 log in SED transect) the coeval deposits are 18 m thick. This suggests a thinning trend from the inner ramp deposits in the SW to the middle-outer ramp deposits in the NE. In many other areas, however, the ramp deposits are characterized just by sediments of the lower subsequence (1a), being the overlying subsequence (1b) non-deposited or eroded. Therefore, due to this limitation (incomplete successions), the observed NE thinning trend cannot be correctly modeled and visualized.

On the contrary, the model reconstructs in detail the different evolutionary steps of the platform depositional geometries. During the early stages of platform growth, the development of a subtle topography, interpreted as an incipient platform margin by Benisek et al. (2009b), is recorded by the increase in thickness of the deposits of subsequences 2a, 2b, 2c, and 2d, from the inner to middle platform settings (Fig. 7). This thickening is followed by a thinning of these sediments basinward (SE). It must be mentioned that, due to the limited exposure of the distal platform deposits in the study area and the relative scarce measurements, the basinward thinning trend could be exaggerated. The steepening of the depositional profile that occurred during the latest stage of the platform evolution is also reproduced by the DOM. The model shows a clear thickening of subsequence 2e towards the platform margin and the occurrence of a clear slope break (Fig. 7). A thinning trend from upslope (subsequence 2e in Fig. 7) to downslope areas (subsequence 2e in Fig. 8) is also reproduced.

In regard to the stratigraphic evolution of the whole studied system, the model reconstruction permits to identify an aggradational pattern during the ramp stage followed by aggradation and progradation towards the SE as the incipient platform margin starts to form (Fig. 6). Progradation becomes the major depositional pattern during the latest stage of platform evolution with steep clinofolds prograding basinward (SE) for more than 1 km, with aggradation being irrelevant (Figs. 8, 10).

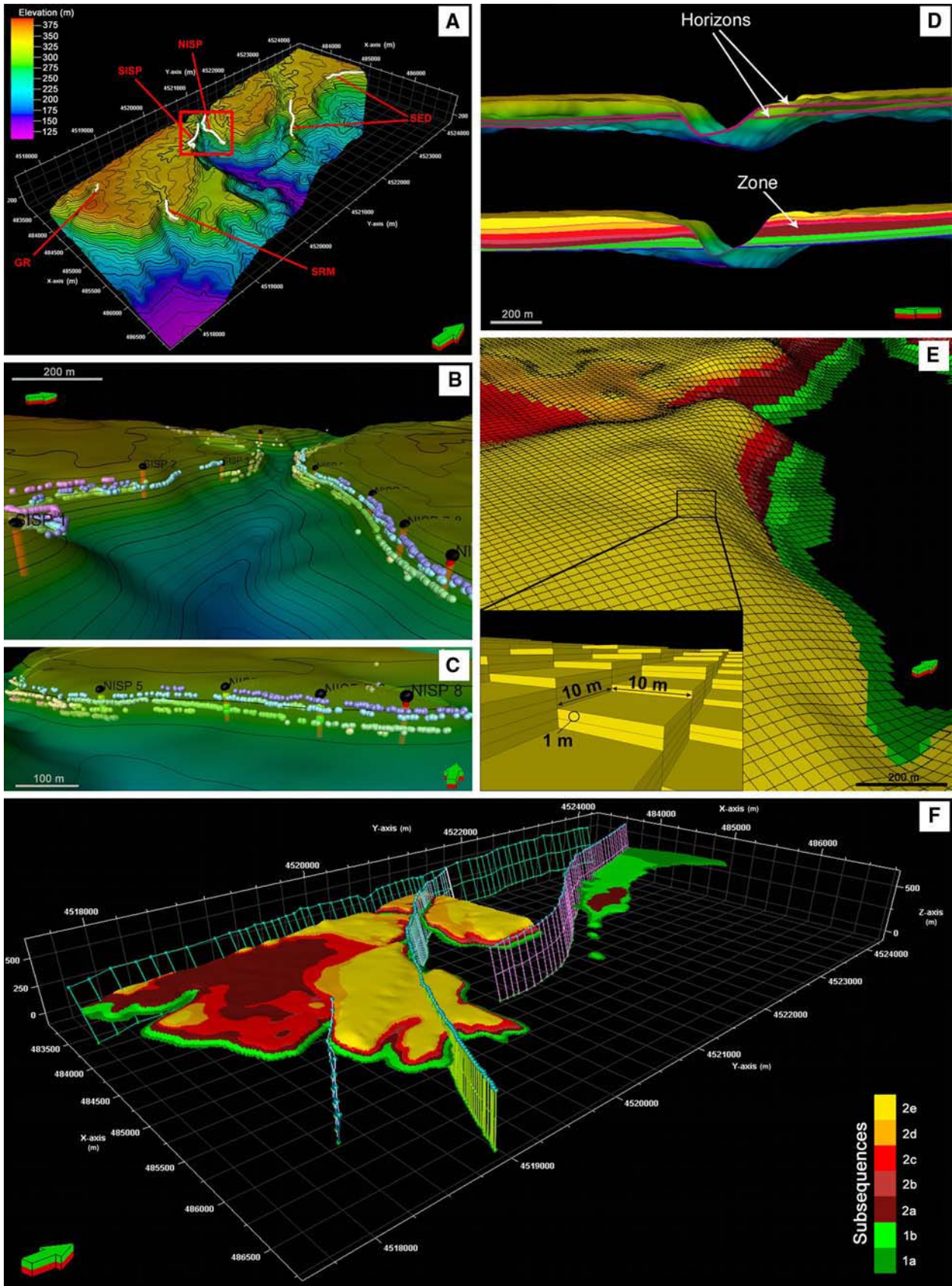
Facies partitioning: digital model versus outcrop data

The generated facies model visualizes the spatial distribution of the facies associations in the studied carbonate system. To test the model reliability, the facies distribution in the outcrop study windows is compared to the distribution reproduced by the model. For this purpose, three study windows recording the most complete successions (NISP, SISP, and SRM transects) have been selected. The comparison between the outcrop data and the model shows that between two tested algorithms, SIS provides the closest match between real and virtual data (Figs. 6, 7, 8) whereas TGS seems to be not so geologically reliable.

Fig. 4 Workflow of geocellular modeling. **a** 3D view of the study area showing the DEM and the locations and transects used as the basis for this model (SED Sedini, NISP North Ispilunca, SISP South Ispilunca, SRM Sa Rocca Manna, and GR Grotta Su Coloru). **b** Close-up view showing the distribution of measured data points merged with the DEM in the Ispilunca transects (for location see box in **a**). The same color is assigned to a set of points measured in the same key stratigraphic boundary. Positions of the logs are indicated with black points. **c** Close-up view showing the measured logs of the Northern Ispilunca (NISP) transect. Note the intersection of the logs with the different stratigraphic boundaries. Data points along the boundaries are also depicted. **d** 2D intersection plane showing the generated horizons (top) and zones (bottom). For visualization purposes, the DEM is displayed. **e** 3D view of the geocellular model showing the cell dimensions; each cell is 10 m × 10 m × 1 m (X, Y, Z). **f** 3D view of the geocellular model showing the faults of the study area and the reconstructed stratigraphic architecture of the carbonate system. For visualization reasons cells are not depicted. Vertical exaggeration = 2 in **a** and **d**

Vertical facies variations are confidently captured by the model since these parameters are directly extracted from the upscaled logs imported in the model. However, in one occasion, a particular facies association (FA7 in SRM 2 in Fig. 5) was not represented in the model because its thickness was below the resolution of the vertical cell size (1 m; Fig. 8). The lateral facies proportion and distribution show to be the most difficult parameter to assess. This can only be modeled with a high degree of confidence obviously when lateral facies changes can be observed in the field or when logged sections are close to each other. Figures 6, 7, and 8 show the model reconstruction of three study windows (NISP, SISP, and SRM transects, respectively) and their good match with the outcrop observations, permitting therefore to assess the quality of the model.

On the contrary, the evaluation of facies distribution in areas away from the study windows is very challenging. For this purpose, three different depositional slices were evaluated: the top of subsequence 1a (ramp), and the top of subsequences 2a and 2e (platform) (Fig. 9a–c). Across the ramp profile, the facies are patchy distributed with no clear depositional meaning due to the limited dataset (Fig. 9a), whereas the modeled facies distribution in the platform seems to be more consistent with the field observations (Fig. 9b, c). The middle platform deposits (FA5) of subsequence 2a extend in most of the study area, whereas the outer platform deposits (FA9) occur just along both margins of the Ispilunca valley (N part of the study area; Fig. 9b). The distribution of coralline red algal bindstones (FA4), which locally form lenses in the FA5 (explained above), is also shown in the model. However, the real extension of FA4 seems to be overestimated. In fact, the largest lenses measured in the outcrops extend up to 200 m, whereas the model shows lengths of ~900 m (green color in Fig. 9b). This feature is believed to be an interpolation artefact due to the few imported logs where this facies has



been observed. Figure 9c shows the facies distribution of the top of subsequence 2e. Platform top deposits (FA6) change basinward (SE) into upper slope deposits (FA7), which pass distally into rhodolitic clinofolds forming the slope (FA8). Some artefacts generated by the model can be observed: e.g., little patches of slope deposits (in purple

and red in Fig. 9c) occurring in between the platform top deposits (in grey in Fig. 9c).

Discussion

Sedimentological implications of the model reconstructions

The digital outcrop model permits to characterize quantitative sedimentologic features in a fixed spatial framework, providing the basis for additional sedimentologic interpretations. By reconstructing the continuity of the studied outcrops in the model, the trend of progradation and the extension of the progradation front of the studied platform have been investigated. The length of the front, between the first clinofolds (SE of SISP transect; Fig. 7) and the last ones measured in the field (SRM transect; Fig. 8), is about 1.5 km. This distance has been calculated by measuring straightforward from the model (Fig. 10). The vertical offset estimated between the slope breaks of these two areas is about 5 m (see isopach lines in Fig. 10). Considering that the succession is not tectonically tilted, a 5-m-vertical offset over a distance of 1.5 km suggests an insignificant aggradation component in the platform (10 cm/30 m). On the contrary, a rapid progradation of the platform is suggested. Nannoplankton data (upper NN4—lower NN5 biozones) and Sr isotope ages (see Benisek et al. 2009a, and references therein) suggest that the studied successions have been deposited in a time interval of 1 to maximum 2 Ma. This results in progradation rates ranging from 750 m/Ma (minimum rate) to 1,500 m/Ma (maximum rate), which are relevant even though not as rapid as those calculated by Maurer (2000) in Rosengarten platform in the Dolomites (~2,700 m/Ma). The significant progradation and the minor aggradation of the Sedini platform suggest deposition under conditions where the sediment production exceeded the space of accommodation in this platform, attributed to the

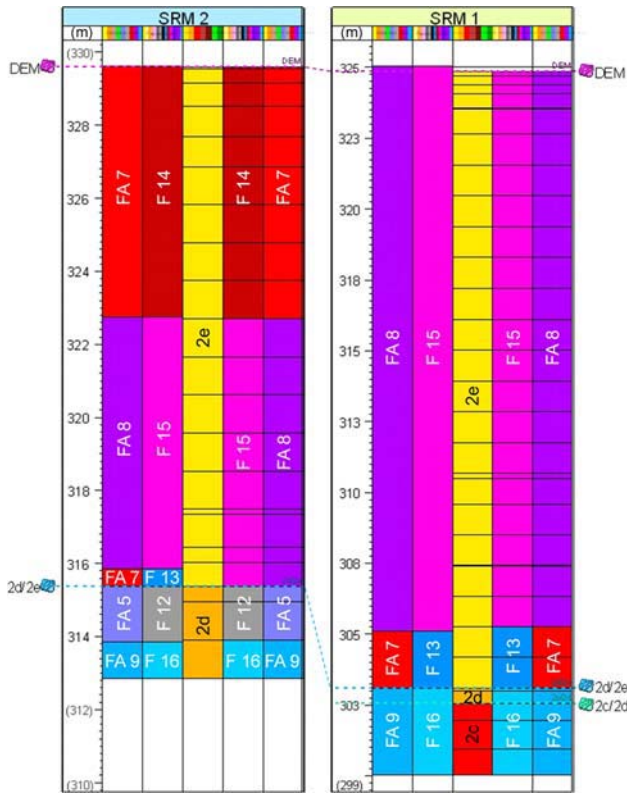


Fig. 5 Upscaling log process. The window shows the comparison between the SRM 2 (left) and SRM 1 (right) outcrop logs and the upscaled logs in terms of facies associations (FA), facies types (F) of Benisek et al. (2009b), and subsequences/model zones. The vertical facies proportions used to generate the model are directly extracted from the upscaled logs. Note that FA7 occurs in the SRM 2 log but is not represented in the model. See text for further discussion

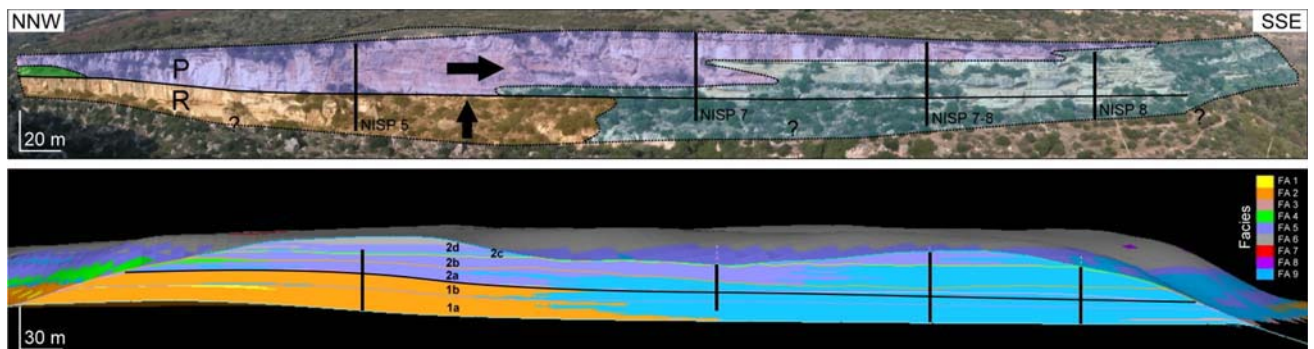


Fig. 6 Northern Ispilunca transect (NISP). Top photo panorama showing the facies distribution observed in the outcrop. Modified after Benisek et al. (2009b). Bottom cross section showing the facies distribution reconstructed by the 3D model in the NISP transect. The

arrows show the ramp (R) aggradation and the platform (P) progradation basinwards. The positions of the measured logs are indicated

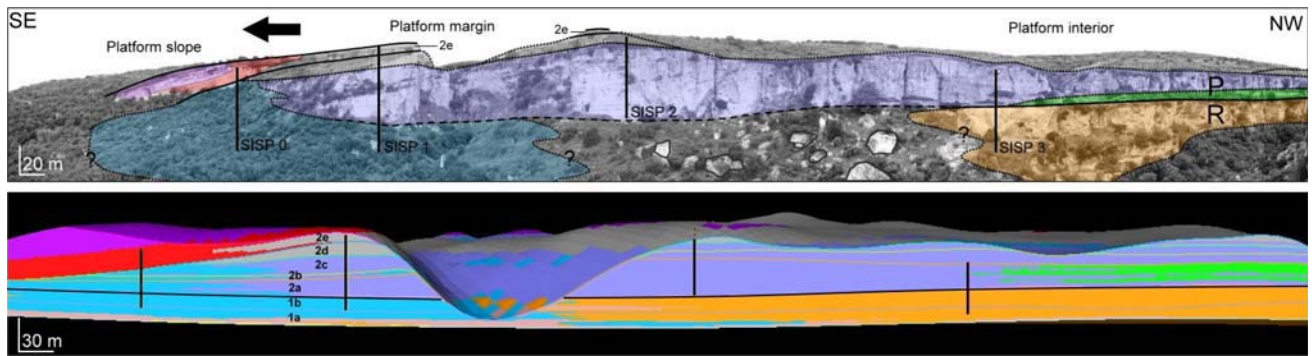


Fig. 7 Southern Ispilunca transect (*SISP*). *Top* photo panorama showing the facies distribution observed in the outcrop. Modified after Benisek et al. (2009b). *Bottom* cross section showing the facies distribution reconstructed by the 3D model in the *SISP* transect. Note

the steepening and thickening of the subsequence 2e from the platform margin and the direction of progradation of the platform basinwards. The positions of the measured logs are indicated. *R* ramp succession, *P* platform succession. For legend of facies associations (*FA*) see Fig. 8

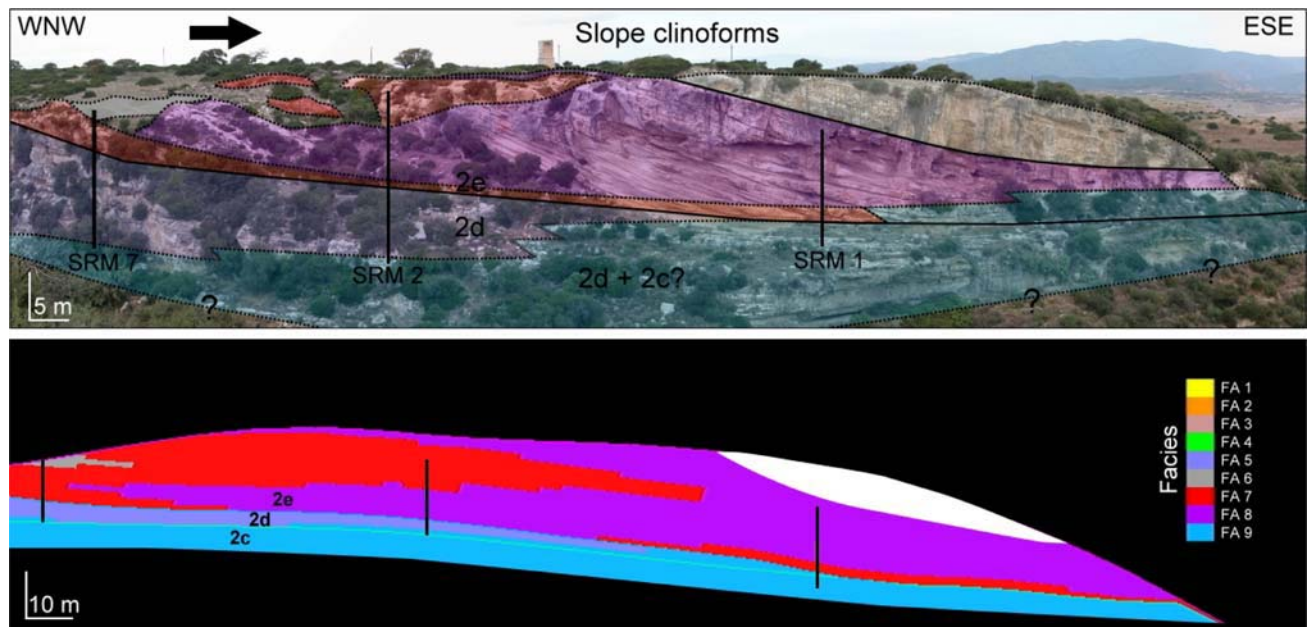


Fig. 8 Sa Rocca Manna transect (*SRM*). *Top* photo panorama showing the facies distribution observed in the outcrop in the latest stage of platform evolution. Modified after Benisek et al. (2009b). Note the slope clinofold beds in the subsequence 2e and the progradation trend of the platform basinwards. *Bottom* cross section

showing the facies distribution reconstructed by the 3D model in the *SRM* transect. The positions of the measured logs are indicated. The deposits overlying the subsequence 2e are not studied in this work and are colored in *white*

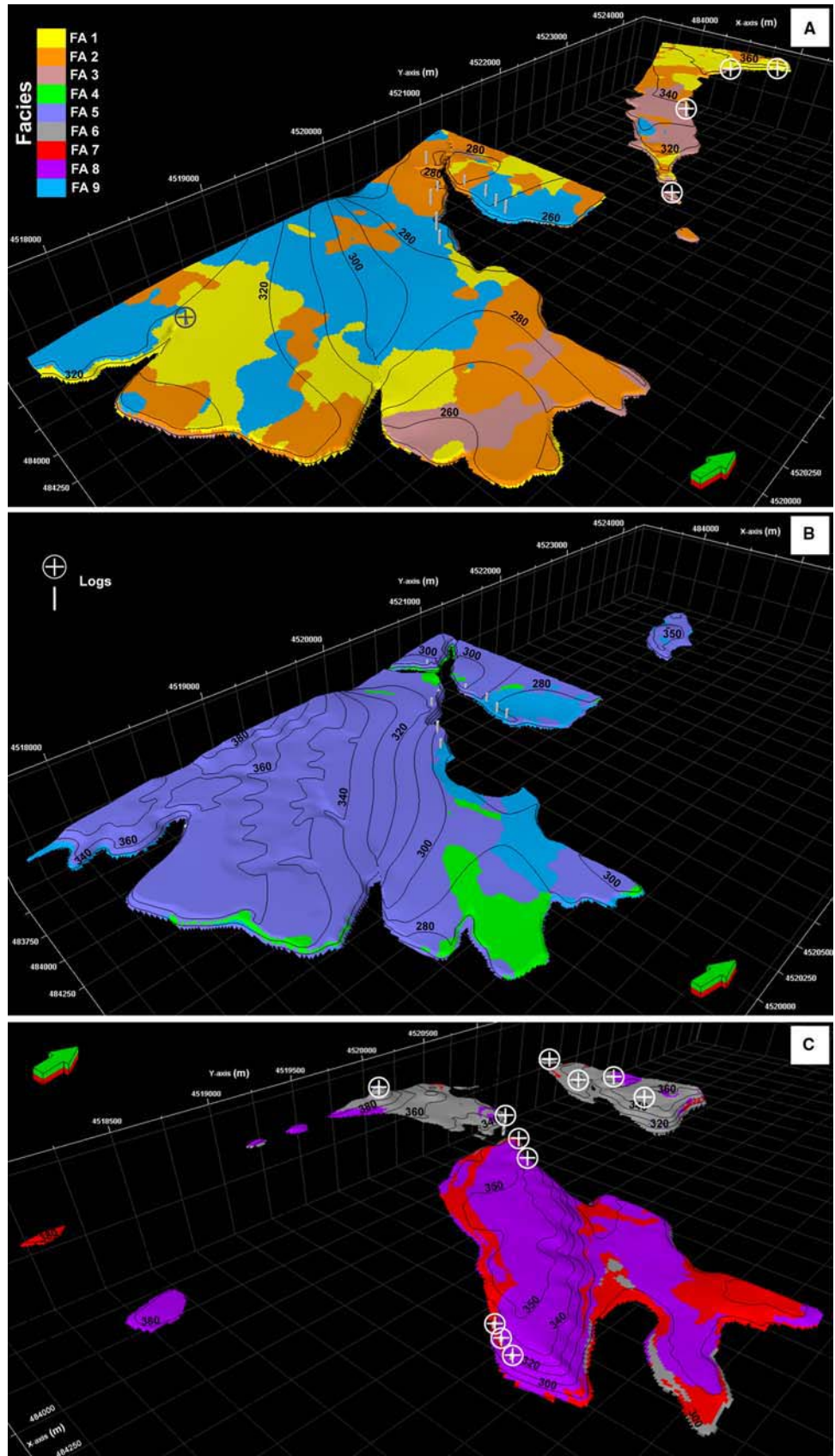
establishment of the tropical factory during the latest stage of platform evolution (Benisek et al. 2009a, 2009b). The flat toplap geometry of the clinofold beds suggests deposition during a sea-level stillstand or a late highstand.

Unlike the depositional geometry model, which generates valuable information at the regional scale, the facies model provides results that seem reliable only in those areas with well-constrained datasets. In fact, although the quality of single outcrop faces is exceptionally good, the control over facies changes in between these single outcrop faces is not. In other words, the limited lateral control on facies distribution makes it difficult to check in detail the

reliability of the facies partitioning in the regional framework. The patchy facies distribution observed sometimes across the studied area might be attributed either to spread datasets or to the used algorithms, which extend the distribution of the different facies to the areas where data are very scarce or absent according to the topography (Fig. 9a, c).

Additionally, the pre-existing topography of the Sedin Limestone Unit (Sowerbutts 2000), evidenced by the variations in thickness of the subsequence 1a (SED and GR transects) and the underlying conglomerates, could exert a role in the complex and inhomogeneous facies distribution across the studied carbonate platform.

Fig. 9 3D views of the facies model showing the facies proportions and distributions across different depositional slices. **a** Plan view of the top of subsequence *1a* (ramp). **b** Plan view of the top of subsequence *2a* (early stage of platform evolution). **c** Plan view of the top of subsequence *2e* (latest stage of platform evolution). Note the locally exposed deposits overlying the studied carbonate succession in the SRM transect (in *white* in Fig. 8) are not depicted. Vertical exaggeration = 2



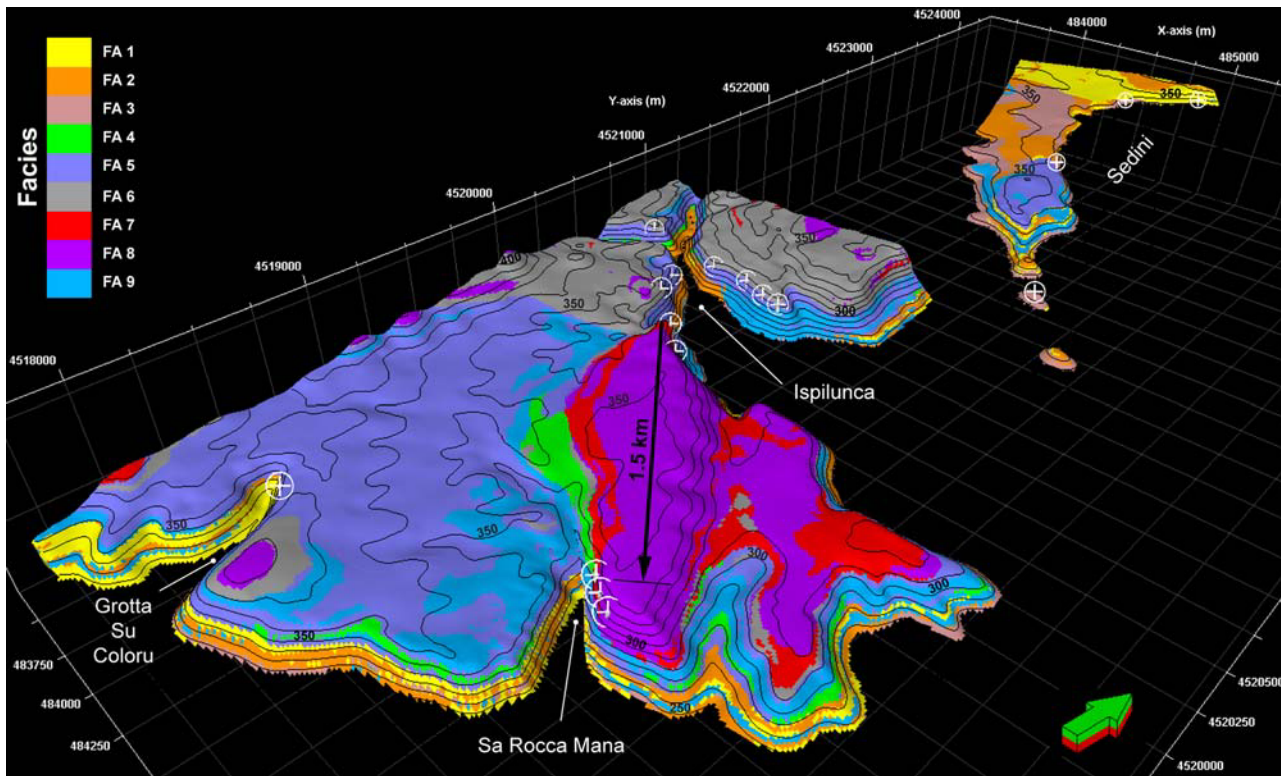


Fig. 10 3D view of the final facies model showing facies proportions and distributions across the studied area. The *arrow* represents the length of the progradation front (1.5 km) measured between the first slope break and the last slope break observed in the field. The vertical offset estimated

between these two areas is 5 m (340 and 345 m, respectively). The location of the studied transects and the positions of the measured logs are indicated. The deposits overlying the studied carbonate succession locally exposed in the SRM transect (in *white* in Fig. 8) are not depicted

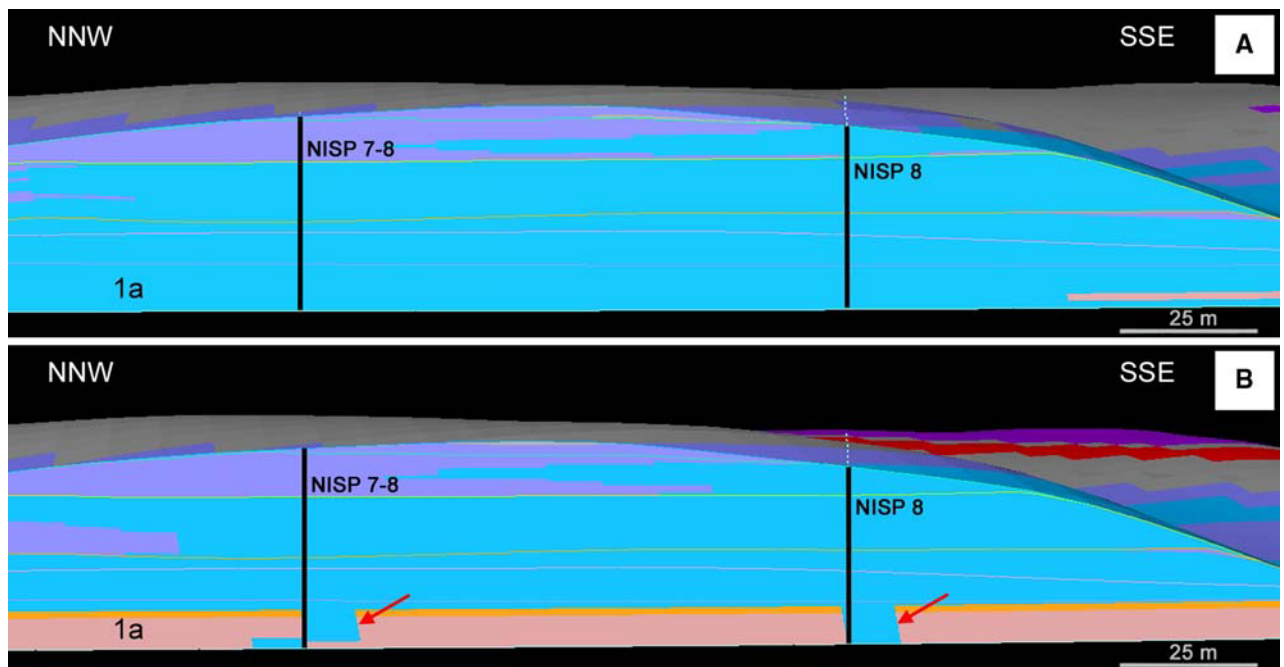


Fig. 11 Model realizations illustrating facies proportions and distributions using two different model algorithms for the SSE part of the NISP outcrop face (see Fig. 6 for location). **a** Cross section of the model created with Sequential Indicator Simulation (SIS). **b** Cross

section of the model created with Truncated Gaussian Simulation (TGS). Note the changes in lateral facies distribution and the abrupt lateral facies changes obtained with the TGS representation (*arrows*). For legend of facies associations (FA), see Fig. 10

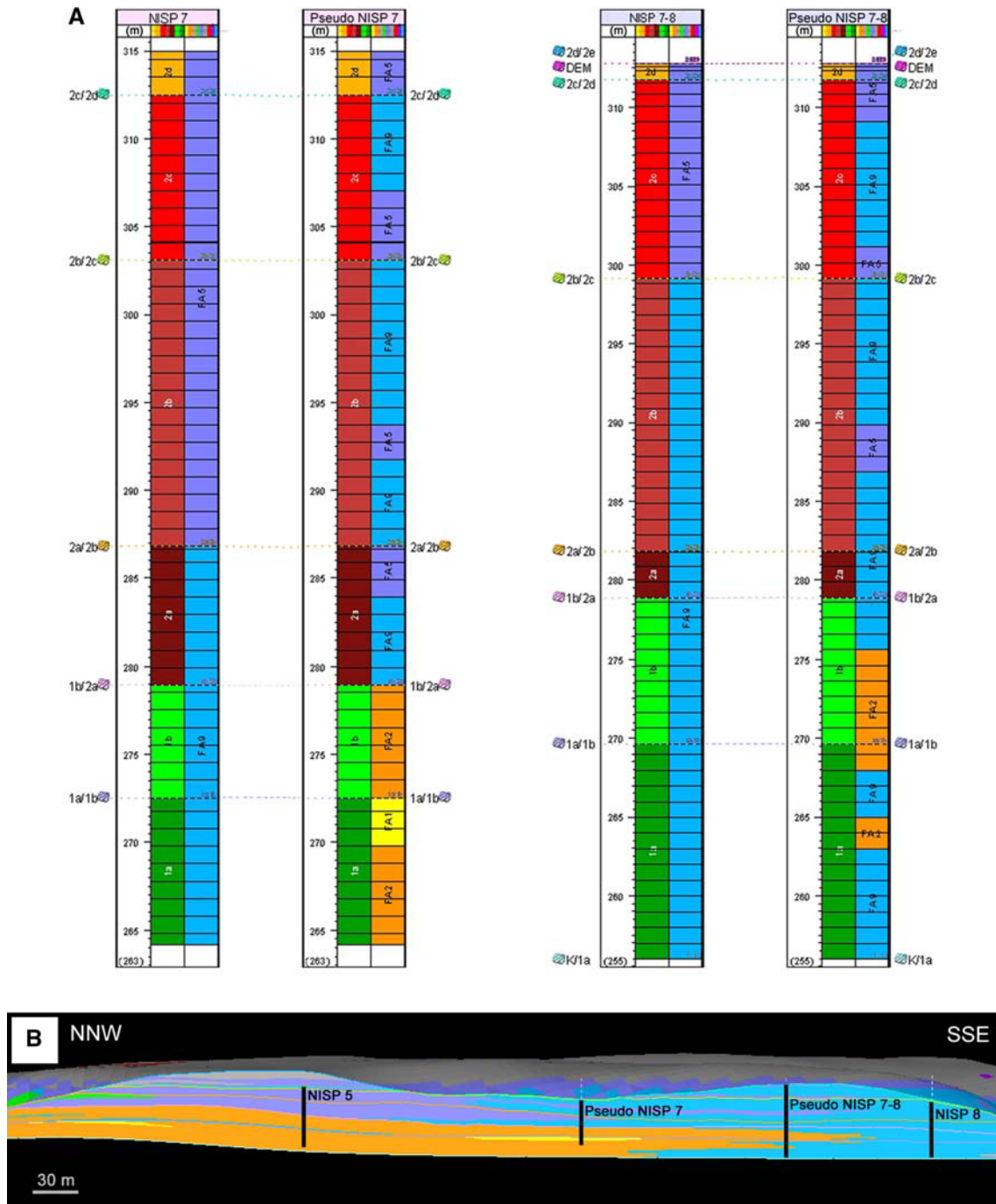


Fig. 12 Evaluation of the modeling algorithm. **a** Comparison between original outcrop logs (NISP 7 and NISP 7–8; see Fig. 6 for location) and pseudo-logs (Pseudo NISP 7 and Pseudo NISP 7–8) showing the different vertical facies proportions and distributions. **b** Cross section of the NISP outcrop face illustrating facies proportions and distributions

reproduced by a second model realization where just two logs were used to condition the model (NISP 5 and NISP 8). Note the changes in lateral and vertical facies proportions and variations with respect to the original model representation and the outcrop observations illustrated in Fig. 6. See text for further discussion

Model methodology

The two different methods used to generate the model (TGS and SIS) were tested by comparing the facies distribution reconstructed by the model with the outcrop

observations (logs NISP 7–8 and NISP 8 in the NISP transect; Fig. 6). The model realization using the SIS algorithm shows a good match with the outcrop data (Figs. 11a, 6). On the contrary, the model using TGS (Fig. 11b) does not match so closely with the outcrop data

and reproduces the facies proportions and distributions only at the discrete positions intersected by the logs (Figs. 11b, 6). Subsequence 1a consists of FA9 (turquoise color) from the central part of the NISP transect (NISP 7) to the southeast, as is reproduced by the SIS model (Fig. 6). However, the model realization using TGS illustrates the FA9 (turquoise color) passing laterally into the FA2 and the FA3 (Fig. 11b). Moreover, it is important to observe that the lateral changes between the different facies associations are very abrupt and not geologically reasonable (see arrows in Fig. 11b). Consequently, the final facies model was realized using the SIS algorithm, which reproduces more reliably the conditioning outcrop data.

In order to quality control the final facies model, the facies proportions and distributions from the input data and the final model are compared at the discrete locations where the original logs are. Since the model is highly constrained by log data, it is expected that the input facies proportions and distributions are similar to those observed in the final model (Figs. 6, 7, 8). Additionally, it is also possible to assess how the modeling algorithm populates the facies laterally (away from log locations) by creating new “pseudo-logs”. These pseudo-logs were created at the same positions of their equivalent original logs, after removing the latter. By using the data analysis tool, information of the facies distribution in the final model at these locations was extracted. Figure 12a illustrates how the facies distribution varies between the original outcrop logs and the “pseudo-logs” in the NISP outcrop face. The facies distribution reproduced by these logs (Fig. 12b) is assessed by comparing the results with the field data (Fig. 6). The observed variation is related to small changes in lateral facies distribution. These changes are related to the random algorithm used to populate the facies laterally within each zone. Application of different modeling techniques (i.e., variograms, trend surfaces) can highly improve the accuracy of the lateral distribution of facies.

Conclusions

Spatial data, measured with a DGPS surveying system, have been linked to an outcrop study allowing the creation of a digital outcrop model for transitional carbonates of the Miocene of northern Sardinia. The studied outcrops are of good quality and have permitted to interpret the main stratigraphic and sedimentologic features across a regional framework. The generation of a digital outcrop model has improved the continuity of the limited exposure of individual outcrops, permitting to reconstruct the basin geometry and facies heterogeneity of the carbonate system in a regional framework. Although the complexity of this fault-block carbonate system, with different strike and dip

depositional directions, the digital outcrop model visualizes the change of the platform depositional profile, from a ramp into a steep-flanked platform. The present work highlights the usefulness of 3D models for reconstructing geometries that cannot be observed straightforward in the field. Moreover, the model has permitted to quantitatively characterize the extension and rates of progradation of the Sedin carbonate platform during its latest evolutionary stage. The extension of the progradation front has a minimum length of 1.5 km, suggesting relatively rapid rates of progradation, ranging from minimum values of 750 m/Ma to maximum values of 1,500 m/Ma. The 3D facies model shows the facies distribution related to each of the stages of platform evolution, showing the change in the type of carbonate factory. The resulting facies model shows a good match with the complex spatial distribution observed in the studied outcrop sectors. Spatially, the detailed facies model helps us to better understand the lateral facies distribution between discrete locations (areas between the outcrop logs) and to predict, to some extent, lateral facies distribution. This model establishes a first approach to further characterize subsurface analogues and to calculate facies volumes. The presented digital outcrop model constitutes a checking loop that allows to test and to improve the observations made in the field, being a unique tool able to show features that are not immediately recognized in the outcrops.

Acknowledgments This research was funded by the Deutsche Forschungsgemeinschaft (Mu 1680/6-1 and Be 1272/12). For discussion on digital outcrop modeling, Jhosnella Sayago (Potsdam) and Iván Fabuel-Pérez (Exxon-Mobil) are thanked. Gianluca Frijia (Potsdam) is acknowledged for stimulating discussions. André Freiwald, Jeroen Kenter, and an anonymous reviewer are thanked for detailed and constructive comments.

References

- Adams EW, Schröder S, Grotzinger JP, McCormick DS (2004) Digital reconstruction and stratigraphic evolution of a microbial-dominated, isolated carbonate platform (terminal Proterozoic, Nama Group, Namibia). *J Sediment Res* 74:479–497
- Adams EW, Grotzinger JP, Watters WA, Schröder S, McCormick DS, Al-Siyabi HA (2005) Digital characterization of thrombolite-stromatolite reef distribution in a carbonate ramp system (terminal Proterozoic, Nama Group, Namibia). *AAPG Bull* 89:1293–1318
- Asprion U, Westphal H, Nieman M, Pomar L (2008) Extrapolation of depositional geometries of the Menorcan Miocene carbonate ramp with ground penetrating radar. *Facies* 55:37–46
- Bellian JA, Kerans C, Jennette DC (2005) Digital outcrop models: application of terrestrial scanning lidar technology in stratigraphic modelling. *J Sediment Res* 75:166–176
- Benisek MF (2008) Facies and stratigraphic architecture of two early Miocene fault-block carbonate platforms in North Sardinia. Unpublished PhD Thesis, Universität Hamburg, p 145
- Benisek MF, Betzler C, Marcato G, Mutti M (2009a) Coralline-algal assemblages of a Burdigalian platform-slope: implications for

- carbonate platform reconstruction (northern Sardinia, western Mediterranean Sea). *Facies* 55:375–386
- Benisek MF, Marcano G, Betzler C, Mutti M (2009b) Facies and stratigraphic architecture of a Miocene warm-temperate to tropical fault-block carbonate platform in Sardinia (central Mediterranean Sea). In: Evolution of carbonate systems during the Oligo-Miocene climatic transition. IAS special publication of the ESF LESC exploratory workshop, Potsdam 2005 (in press)
- Betzler C, Brachert TC, Braga JC, Martín JM (1997) Nearshore, temperate, carbonate depositional systems (Lower Tortonian, Agua Amarga Basin, southern Spain): implications for carbonate sequence stratigraphy. *Sediment Geol* 113:27–53
- Betzler C, Martín JM, Braga JC (2000) Non-tropical carbonates related to rocky submarine cliffs (Miocene, Almería, southern Spain). *Sediment Geol* 131:51–65
- Bosence DWJ (2005) A new, genetic classification of carbonate platforms based on their basinal and tectonic setting in the Cenozoic. *Sediment Geol* 175:49–72
- Bosence DWJ, Cross NE, Hardy S (1998) Architecture and depositional sequences of Tertiary fault-block carbonate platforms; an analysis from outcrop and computer modeling. *Mar Petrol Geol* 15:203–211
- Brachert TC, Betzler C, Braga JC, Martín JM (1996) Record of climatic change in neritic carbonates: turnover in biogenic associations and depositional models (Late Miocene, southern Spain). *Geol Rundsch* 85:327–337
- Brachert TC, Betzler C, Braga JC, Martín JM (1998) Micro-taphofacies of a warm-temperate carbonate ramp (upper Miocene, S-Spain). *Palaios* 13:459–475
- Brandano M, Corda L (2002) Nutrients and tectonics: constraints for the facies architecture of a Miocene carbonate ramp in central Italy. *Terra Nova* 14:257–262
- Brandano M, Vannucci G, Pomar L, Obrador A (2005) Rhodolith assemblages from the lower Tortonian carbonate ramp of Menorca (Spain): environmental and palaeoclimatic implications. *Palaeogeogr Palaeoclimatol Palaeoecol* 226:307–323. doi: [10.1016/j.palaeo.2005.04.034](https://doi.org/10.1016/j.palaeo.2005.04.034)
- Cherchi A, Montadert L (1982) Oligo-Miocene rift of Sardinia and the early history of the Western Mediterranean Basin. *Nature* 298:736–739
- Clark JD, Pickering KT (1996) Submarine channels, processes and architecture. Vallis Press, London
- Enge HD, Buckley SJ, Rotevatn A, Howell JA (2007) From outcrop to reservoir simulation model: workflow procedures. *Geosph* 3:469–490
- Esteban M (1996) An overview of Miocene reefs from Mediterranean areas: general trends and facies models. In: Franseen EK, Esteban M, Ward WC, Rouchy JM (eds) Models for carbonate stratigraphy from Miocene reef complexes of Mediterranean regions, concepts in sedimentology and palaeontology, vol 5. SEPM, Tulsa, pp 3–53
- Fabuel-Perez I (2008) 3D reservoir modeling of Upper Triassic continental fluvial systems. Integration of digital outcrop models with high-resolution sedimentology: Central High Atlas, Morocco. Unpublished PhD Thesis, University of Manchester, p 300
- Falivene O, Arbues P, Gardiner A, Pickup G, Muñoz JA, Cabrera L (2006) Best practice stochastic facies modeling from a channel-fill turbidite sandstone analog (the Quarry outcrop, Eocene Ainsa Basin, northeast Spain). *AAPG Bull* 90:1003–1029
- Grammer GM, Harris PM, Eberli GP (2004) Overview with examples from the Bahamas. In: Grammer GM (ed) Integration of outcrop and modern analogs in reservoir modeling, vol 80. AAPG Memoir, Houston, pp 1–22
- Halfar J, Godinez-Orta L, Mutti M, Valdez-Holguin J, Borges J (2004) Nutrient- and temperature controls on modern carbonate production: an example from the Gulf of California, Mexico. *Geology* 32:213–216
- Jones RR, McCaffrey KJW, Imber J, Wightman R, Smith SAF, Holdsworth RE, Clegg P, De Paola N, Healy D, Wilson RW (2007) Calibration and validation of reservoir models: the importance of high-resolution, quantitative outcrop analogues. In: Griffith P et al (eds) The future of geological modelling in hydrocarbon development. *Geol Soc Spec Publ*, Tulsa, p 13
- Marcano GH (2008) Investigation on sedimentology and early diagenesis in shallow-water warm-temperate to tropical Miocene carbonates: a case study from northern Sardinia, Italy. Unpublished PhD Thesis, Universität Potsdam, p 99
- Martín JM, Braga JC, Betzler C, Brachert TC (1996) Sedimentary model and high-frequency cyclicity in a Mediterranean, shallow shelf, temperate carbonate environment (uppermost Miocene, Agua Amarga Basin, southern Spain). *Sedimentology* 43:263–277
- Maurer F (2000) Growth mode of Middle Triassic carbonate platforms in the Western Dolomites (Southern Alps, Italy). *Sediment Geol* 134:275–286
- Mutti M, Bernoulli D, Stille P (1997) Temperate platform drowning episodes are linked to Miocene oceanographic events: Maiella platform margin, Italy. *Terra Nova* 9:122–125
- Mutti M, Bernoulli D, Spezzaferri S, Stille P (1999) Lower and Middle Miocene carbonate facies in the central Mediterranean: the impact of paleoceanography on sequence stratigraphy. In: Harris PM, Saller AH, Simo JA (eds) Advances in carbonate sequence stratigraphy: application to reservoirs, outcrops and models, vol 63. *Soc Sediment Geol Spec Publ*, Tulsa, pp 371–384
- Pomar L, Hallock P (2008) Carbonate factories: a conundrum in sedimentary geology. *Earth Sci Rev* 87:134–169
- Pomar L, Kendall CGSC (2007) Architecture of carbonate platforms: a response to hydrodynamics and evolving ecology. In: Lukasik J, Simo A (eds) Controls on carbonate platform and reef development, vol 89. *SEPM Spec Publ*, Tulsa, pp 187–216
- Pomar L, Brandano M, Westphal H (2004) Environmental factors influencing skeletal grain sediment associations: a critical review of Miocene examples from the western Mediterranean. *Sedimentology* 51:627–651
- Pringle JK, Howell JA, Hodgetts D, Westerman AR, Hodgson DM (2006) Virtual outcrop models of petroleum reservoir analogues: a review of the current state-of-the-art. *First Break* 24:33–41
- Redfern J, Hodgetts D, Fabuel-Perez I (2007) Digital analysis brings renaissance for petroleum geology outcrop studies in North Africa. *First Break* 25:81–87
- Schettino A, Turco E (2006) Plate kinematics of the Western Mediterranean region during the Oligocene and early Miocene. *Geoph J Int* 166:1398–1423
- Sowerbutts A (2000) Sedimentation and volcanism linked to multi-phase rifting in an Oligo-Miocene intra-arc basin, Anglona, Sardinia. *Geol Mag* 137:395–418
- Thomas B, Gennesseaux M (1986) A two-stage rifting in the basins of the Corsica-Sardinian Straits. *Mar Geol* 72:225–239
- Verwer K, Kenter JAM, Maathuis B, Della Porta G (2004) Stratal patterns and lithofacies of an intact seismic-scale Carboniferous carbonate platform (Asturias, northwestern Spain): a virtual outcrop model. In: Curtis A, Wood R (eds) Geological prior information: informing science and engineering, vol 239. *Geol Soc Lond Spec Publ*, Tulsa, pp 29–41
- Verwer K, Adams EW, Kenter JAM (2007) Digital outcrop models: technology and applications. *First Break* 25:57–63
- Warlich GM, Bosence DWJ, Waltham DA (2005) 3D and 4D controls on carbonate depositional systems: a sedimentological and sequence stratigraphic analysis of an attached carbonate platform and atoll (Miocene, Níjar Basin, SE Spain). *Sedimentology* 52:369–383